Biosensors and Bioelectronics 157 (2020) 112157

Contents lists available at ScienceDirect

Biosensors and Bioelectronics

journal homepage: http://www.elsevier.com/locate/bios

Cardiac troponin I photoelectrochemical sensor: {Mo_{368}} as electrode donor for Bi_2S_3 and Au co-sensitized FeOOH composite

Chunzhu Bao [a], Xin Liu [a], Xinrong Shao [a], Xiang Ren [a], Yong Zhang [a], Xu Sun [a], Dawei Fan [a,*], Qin Wei [a], Huangxian Ju [a,b,**]

[a] Key Laboratory of Interfacial Reaction & Sensing Analysis in Universities of Shandong, School of Chemistry and Chemical Engineering, University of Jinan, Jinan, 250022, PR China

[b] State Key Laboratory of Analytical Chemistry for Life Science, School of Chemistry and Chemical Engineering, Nanjing University, Nanjing, 210023, PR China

ARTICLE INFO

Keywords:
Photoelectrochemical
Sensor
{Mo_{368}}
FeOOH
Bi_2S_3
Au
Cardiac troponin I

ABSTRACT

A suitable electron donor, which guarantees the stability of the whole system, is considered as the driving force of the PEC sensor. Nowadays, searching appropriate electron donor is still one of the orientations to explorate in the field of sensor. $Na_{48}[H_{496}Mo_{368}O_{1464}S_{48}]\cdot ca.1000H_2O$ (abbr. {Mo_{368}}), as a type of polyoxometalate, has perfect morphology, definite size and unique electronic property. Due to the prominent water solubility, {Mo_{368}} usually releases small cations and exists as large anions in the ultrapure water. The interesting property endows {Mo_{368}} with excellent reducibility, which provides great feasibility to become an outstanding electron donor. In addition, FeOOH prepared through a simple operation owns high adsorption capacity, which ensures the fastness of other materials. Subsequently, the narrow band-gap of Bi_2S_3 and the unique noble metal properties of Au nanoparticles are utilized to co-sensitize FeOOH to improve the light-harvesting capability and photoelectric conversion efficiency. Combined with the specificity recognition of antigen and antibody, a novel photoelectrochemical sensor is constructed with a wide detection range of 1.00 pg mL^{-1} - 100 ng mL^{-1} and low detection limit (0.76 pg mL^{-1}), which achieves the sensitive detection of cardiac troponin I in early diagnosis of cardiovascular disease.

1. Introduction

Photoelectrochemical (PEC) sensor integrating the advantages of photochemical method and electrochemical technology displays superior peculiarities of simple device, reduced background interference, high sensitivity and excellent stability(Li et al., 2019b; Li et al., 2019f; Lv et al., 2018; Zhou et al., 2018). Under the irradiation of visible light, the excited state of photoactive materials is generated, which accelerates the electron transfer, and then facilitates the output of photocurrent signals (Li et al., 2018; Li et al., 2019e; Saha et al., 2018). Meanwhile, electron donor constantly captures photo-generated holes to ensure the stability of PEC sensor(Bao et al., 2019; Chen et al., 2018; Chi et al., 2019; Gao et al., 2019; Li et al., 2019a), which determines that choosing an appropriate electron donor is significant in the design process of PEC sensor.

As a late-model inorganic macromolecules at the nanoscale, polyoxometalate refers to a group of cluster compound which is composed of polymetallic atoms and heteroatoms in a certain structure and bridged by oxygen atoms. On account of the unique electronic properties and structural diversity, polyoxometalate has measureless potential in material(Adhikary et al., 2018; Wang et al., 2019), catalysis (Guo et al., 2018; Li et al., 2019d), supercapacitors(Wang et al., 2018a), and so on. $Na_{48}[H_{496}Mo_{368}O_{1464}S_{48}]\cdot ca.1000H_2O$ (abbr. {Mo_{368}}), an important type of polyoxometalate, owns fascinating peculiarities such as perfect morphology, constant composition and definite size. Now, it has attracted the attention of many scholars. For example, Achim Müller et al. have researched the simple preparation method and characters of the hedgehog-shaped {Mo_{368}}(Müller et al., 2004). Later, the group has explored the nanochemistry of {Mo_{368}}(Müller et al., 2010). Subsequently, Somenath Garai et al. have analyzed the distinct electronic and structural properties of {Mo_{368}}, and self-assembled intospherical vesicles encapsulated by surfactant(Garai et al., 2015). {Mo_{368}} is an

* Corresponding author.
** Corresponding author. Key Laboratory of Interfacial Reaction & Sensing Analysis in Universities of Shandong, School of Chemistry and Chemical Engineering, University of Jinan, Jinan, 250022, PR China.
E-mail addresses: jndxfandawei@126.com (D. Fan), hxju@nju.edu.cn (H. Ju).

https://doi.org/10.1016/j.bios.2020.112157
Received 27 October 2019; Received in revised form 5 March 2020; Accepted 15 March 2020
Available online 19 March 2020

inorganic macromolecule material that can be easily synthesized, and the most surprising thing is that {Mo_{368}} usually releases small cations and exists as large anions in the ultrapure water because of the prominent water solubility(Garai et al., 2015). Due to the unique electronic property, {Mo_{368}} endows with excellent reducibility, whereby provides a great feasibility to become an outstanding electron donor. Its application in PEC sensor not only enriches the technology in the field of PEC, but also provides a new strategy for the construction of sensor.

If a suitable electron donor is considered as the driving force of the PEC sensor, novel photosensitive materials are the indispensable foundation of the whole sensor system. As a high-profile photosensitive material, iron oxyhydroxide (FeOOH) has boundless prospects in the various fields due to the advantages of low cost, environmental friendliness, excellent photocatalytic activity and so on(Hu et al., 2019; Zhou et al., 2017). For example, Ai et al. have prepared flowerlike α-FeOOH as catalyst to reduce nitro compounds(Ai et al., 2018). Xin et al. have utilized FeOOH nanosheets to enhance the capacitive performance of carbonized wood(Xin et al., 2018). Feng et al. have designed FeOOH/-CeO_2 heterojunction for the oxygen evolution reaction(Feng et al., 2016). Nonetheless, the wide band-gap of FeOOH impedes electron transfer and further reduces the photoelectric conversion efficiency. Fortunately, abundant active hydroxyl groups are distributed on the surface of FeOOH, which endows FeOOH with high adsorption capacity (Wang et al., 2016). Using the unique property, a novel FeOOH/Bi_2S_3 heterojunction is synthesized by growing bismuth sulfide (Bi_2S_3) on the surface of FeOOH in our work.

As one of the most concerned semiconductor nanomaterials, Bi_2S_3 with narrow band-gap is frequently used to sensitize other materials to adjust the band-gap of the materials(Bao et al., 2019; Cao et al., 2018; Chen et al., 2019; Guo et al., 2019; Wang et al., 2018b). And the absorbance coefficient of Bi_2S_3 is about 104 cm^{-1} displaying broad absorption in the visible light spectra(Cui et al., 2018; Li et al., 2019c; Paul et al., 2017). Hence, Bi_2S_3 is attached on the surface of FeOOH by the ion adsorption reaction between OH^- and Bi^{3+}, which obviously improves the charge carrier separation and the mass-transfer ability enhancing the photoelectric conversion efficiency. In addition, combining with noble metal nanoparticles (Au, Ag, Pt) is deemed to an effective approach that promotes electron transfer and boosts the performance of nanomaterials because of the surface plasmon resonance (SPR) effect, outstanding optical stability and excellent quantum yield(Jia et al., 2019; Wen et al., 2019). Kaylyn K. Leung et al. have electrodeposited DNA monolayers on Au and evaluated with fluorescence microscopy to further control the preparation of biosensor surface(Leung et al., 2019). Yuan et al. have used the SPR effect of Au nanoparticles (Au NPs) to detect Hg^{2+}(Yuan et al., 2019). Therefore, Au NPs are absorbed tightly on the FeOOH/-Bi_2S_3 heterojunction due to the band of Au–S, which enhances the light-harvesting capability and promotes the ability of electron transfer of materials.

In our work, a novel PEC sensor based on the matrix of FeOOH/Bi_2S_3/Au is constructed using {Mo_{368}} with unique structure as electron donor for the ultrasensitive detection of cardiac troponin I (cTnI). With the acceleration of aging society, cardiovascular disease has gradually become one of the hot issues in the society. Cardiovascular diseases mainly include hypertension, myocardial infarction, angina pectoris, heart failure and so on, which are critical, acute and severe diseases and lead to an increase in mortality. The concentration of cTnI is significantly different in the serum of normal persons or patients(Sun et al., 2019a; Tan et al., 2017; Welsh et al., 2019). Generally, the content of cTnI in normal human serum is usually below 0.2 ng mL^{-1}. And it implies a direct damage of the myocardium when the concentration of cTnI is higher than 2.0 ng mL^{-1}(Szunerits et al., 2019). Therefore, cTnI is known as one of the biochemical markers of cardiovascular disease (Chapman et al., 2017; Fan et al., 2018a; Lv et al., 2019; Sun et al., 2019b). The ultrasensitive detection of cTnI benefits the early diagnosis of cardiovascular disease.

2. Experimental

2.1. Materials and reagents

Phosphate buffered saline (PBS, 1/15 mol L^{-1} of KH_2PO_4 and 1/15 mol L^{-1} of Na_2HPO_4) containing {Mo_{368}} was used as an electrolyte for the PEC measurements. A 100 W LED lamp of white light was used for an irradiation source and the wavelength range of LED lamp was shown in Fig. S1. And other details about materials and apparatus were displayed in the Supporting Information (SI†).

2.2. Synthesis of FeOOH on the ITO electrode

The FeOOH was formed by the reaction between prussian blue (PB) and NaOH solution. The PB was prepared according to the previous report(Han et al., 2014) and the details were showed in SI†. Then, 0.1 mol L^{-1} of NaOH solution was modified on the ITO/PB electrode for 15 min to generate FeOOH. The above electrode was washed with ultrapure water and dried at room temperature to obtain the ITO/FeOOH electrode.

2.3. Construction of the novel PEC sensor

According to the layer by layer assembly method, the novel PEC sensor was performed for the quantitative detection of cTnI (as depicted in Scheme 1). At first, PB was deposited on the ITO electrode by electrodeposition method. Utilizing the reaction between PB and OH^-, FeOOH was successfully formed and tightly coated on the ITO electrode. Subsequently, the above electrode was steeped in 0.04 mol L^{-1} dimethyl formamide solution of $Bi(NO_3)_3$ for 1 min and rinsed with dimethyl formamide. Due to the adsorption of positive and negative ions, the abundant Bi^{3+} was absorbed on the surface of FeOOH. Then, the electrode was immersed in 0.36 mol L^{-1} of Na_2S solution for another 1 min and thoroughly washed with ultrapure water. After repeated the above procedure for 4 cycles, Bi_2S_3 generated because of the successive ionic layer adsorption and reaction. The above electrode was immersed in the Au NPs solution (the synthesis process of Au NPs solution was showed in the SI†) and oscillated overnight. After washing with ultrapure water, the ITO/FeOOH/Bi_2S_3/Au electrode was obtained. Afterwards, 6 μL anti-cTnI (1 μg mL^{-1}) was incubated on the above electrode for 30 min, and then rinsed to move the uncombined anti-cTnI. In order to block nonspecific sites on the FeOOH/Bi_2S_3/Au composite, 8 μL of bovine serum albumin (BSA, 0.1%) was dropped on the above electrode. After rinsing, various concentrations of cTnI (6 μL) were incubated on the above electrode due to the specific binding of antigens and antibodies. Finally, the prepared ITO/FeOOH/Bi_2S_3/Au/anti-cTnI/BSA/cTnI electrodes were washed and stored for the further use.

3. Results and discussion

3.1. Characterization of the applied materials

The SEM, EDS and TEM images were researched to explore the morphology and component of the applied materials. As displayed in Fig. 1A, the obtained FeOOH was composed of abundant nanoparticles. The large specific surface area of FeOOH possessed excellent load capacity. And the EDS image (Fig. 1G) indicated the component of FeOOH consisting of Fe and O elements. In addition, the abundant active OH^- groups were distributed on the surface of FeOOH, which was further conducive to the absorption of Bi_2S_3. Comparing with the morphology of pure FeOOH, the SEM image of FeOOH/Bi_2S_3 (Fig. 1B) was distinctly prettier. Generated by ion adsorption reaction, Bi_2S_3 displayed unique floral structure forming by the aggregation of numerous nanorods and nanosheets. And the EDS image of FeOOH/Bi_2S_3 (Fig. 1H) concluded Fe, O, Bi and S elements, which proved the successful absorption of Bi_2S_3. Fig. 1C manifested the SEM image FeOOH/Bi_2S_3/Au, and Fig. 1D and E

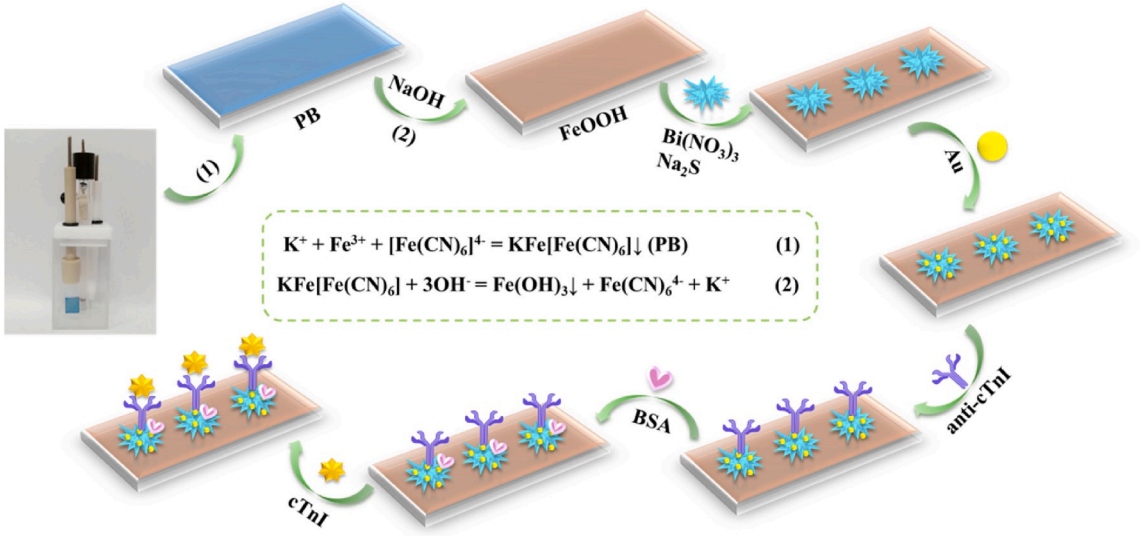

Scheme 1. The construction process of the designed PEC sensor for the quantitative detection of cTnI.

further showed the more legible morphology. It was obvious that a mass of Au NPs was loaded on FeOOH/Bi_2S_3, which was further demonstrated in the EDS image of FeOOH/Bi_2S_3/Au (Fig. 1I). In addition, the TEM image of Au NPs was showed in Fig. 1F indicating the uniform size of Au NPs.

The X-ray diffraction (XRD) patterns of FeOOH (a), FeOOH/Bi_2S_3 (b) and FeOOH/Bi_2S_3/Au (c) were measured and displayed in Fig. 2A. It was obvious that the main diffraction peaks of FeOOH could match well with the standard spectrum of FeOOH (PDF#26-0792). With the modification of Bi_2S_3 and Au, the main diffraction peaks of the obtained materials could be consistent with the standard spectra of Bi_2S_3 (PDF#17-0320) and Au (PDF#04-0784), respectively. The result verified the successful preparation of materials. The fabrication process of FeOOH could be explained as follows. Under the potential of 0.4 V, the substances in solution reacted as equation (1) to form PB that was deposited on the surface of ITO electrode. In an alkaline environment, the PB sediment reacted with OH^- and converted to $Fe(OH)_3$ precipitate according to equation (2). With the gradual accumulation of precipitate, $Fe(OH)_3$ achieved to the critical value and then translated into FeOOH. FeOOH nanoparticles cross-linked through hydrogen bonding, which exposed a mass of surface active OH^- and enhanced the chemical reactivity of FeOOH(Wang et al., 2016). In addition, the band-gap of FeOOH was calculated to be 2.78 eV via the UV–vis diffuse reflectance spectrum (Fig. 2B). And the Mott-Schottky curves (Fig. 2C) of FeOOH were measured to obtain that the conduction band (CB) and valence band (VB) of FeOOH were about 0.59 V and 3.37 V, respectively.

$$K^+ + Fe^{3+} + [Fe(CN)_6]^{4-} = KFe[Fe(CN)_6]\downarrow \text{ (PB)} \quad (1)$$

$$KFe[Fe(CN)_6] + 3OH^- = Fe(OH)_3\downarrow + Fe(CN)_6^{4-} + K^+ \quad (2)$$

The UV–vis diffuse reflectance spectra of FeOOH, FeOOH/Bi_2S_3 and FeOOH/Bi_2S_3/Au were researched to analyze the absorption ability of materials to visible light. It was obvious that the absorption range and intensity of FeOOH/Bi_2S_3/Au to the visible light far exceeded that of FeOOH and FeOOH/Bi_2S_3 in Fig. 2D. The result reflected that Bi_2S_3 and Au NPs co-sensitized FeOOH boosted the utilization rate to the visible light. Moreover, the FT-IR spectrum of {Mo_{368}} (the synthesis process of {Mo_{368}} was shown in SI†) was investigated and indicated in Fig. 2E. The characteristic absorption bands (wavenumber/cm^{-1}) were showed at 1620 (m) ($\delta(H_2O)$), 1190 (w), 1100 (w), 1055 (all represented bidentate SO_4^{2-} ligands), 982 (s) (belonged to Mo═O), 764(s), 702(sh), 628(w) and 558(m). The representative absorption bands were similar to the reported literature(Müller et al., 2004), which also convincingly testified the successful preparation of {Mo_{368}}. After filling with nitrogen for 20 min, the cyclic voltammograms (CV) response was measured to analyze the redox property of {Mo_{368}}, and the data were shown in Fig. 2F. It was obvious that the CV curve of ITO electrode had no redox peak at all if pure PBS solution was used as the electrolyte (curve a). However, the measured CV curve of ITO electrode had distinct oxidation peaks (at 0.039 V and 0.27 V) and reduction peak (at 0.18 V) when the PBS solution containing {Mo_{368}} was designed as electrolyte (curve b), which strongly proved the excellent redox property of {Mo_{368}}.

3.2. Characterization of constructed PEC sensor

Fig. 3 demonstrated the photocurrent response and electrochemical impedance spectroscopy (EIS) to testify the construction process of PEC sensor. As shown in Fig. 3A and B, the photocurrent signal of pure ITO electrode was nearly 0 μA (curve a). With the modification of FeOOH (curve b), Bi_2S_3 (curve c) and Au NPs (curve d), the photocurrent signal gradually improved due to the excellent conductivity of materials. And the signal of ITO/FeOOH/Bi_2S_3/Au electrode achieved the maximum (about 31 μA) indificating the excellent PEC performance of FeOOH/Bi_2S_3/Au. Subsequently, the outstanding insulation of anti-cTnI (curve e), BSA (curve f) and cTnI (curve g) inhibited electron transfer, which led to the gradual decrease of photocurrent intensity. As shown in Fig. 3C, the semicircle part in EIS Nyquist plots was equivalent to the charge transfer resistance (R_{et}) value reflecting the electron transfer resistance on the surface of ITO electrode. And the relevant simulation parameters of the equivalent circuit components were displayed in Table S1. The R_{et} value of ITO electrode (curve a) was minimum (10.47 Ω). After modifying with FeOOH (curve b) and Bi_2S_3 (curve c), the R_{et} values became to 12.48 Ω and 29.88 Ω, respectively. Afterwards, the R_{et} value became to 17.30 Ω due to the loading of Au NPs with excellent conductivity (curve d). As the modification of anti-cTnI (curve e), BSA (curve f) and cTnI (curve g), the R_{et} values gradually increased to 47.17 Ω, 53.52 Ω and 76.03 Ω. The result implied that the resistance on the surface of ITO electrode increasingly enhanced, which demonstrated the successful construction of the PEC sensor.

The electron transfer mechanism of constructed PEC sensor was shown in Fig. 3D. According to the previous reported work, the CB and VB were about 0.12 V and 1.76 V, respectively(Fan et al., 2018b). And the narrow band-gap of Bi_2S_3 (1.64 eV) was beneficial to the electron transfer(Fan et al., 2018b). With the visible light as excitation light source, the electrons absorbed light energy and then transferred from VB to CB of Bi_2S_3. The perfect match of band-gap between Bi_2S_3 and FeOOH

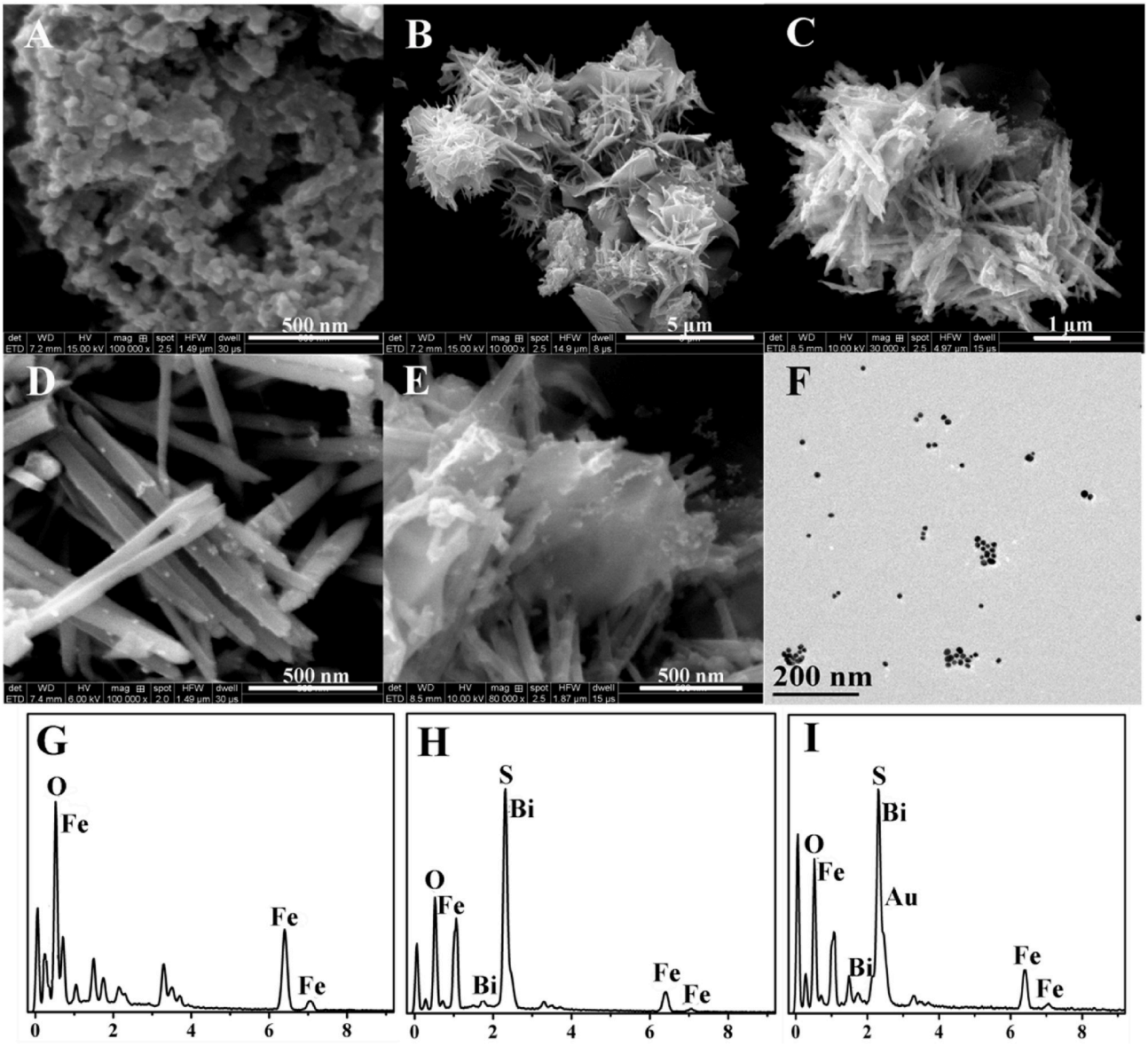

Fig. 1. SEM images of FeOOH (A), FeOOH/Bi_2S_3 (B) and FeOOH/Bi_2S_3/Au (C). Magnified SEM images of FeOOH/Bi_2S_3/Au (D and E). TEM image of Au NPs (F). EDS images of FeOOH (G), FeOOH/Bi_2S_3 (H) and FeOOH/Bi_2S_3/Au (I).

accelerated the photo-generated electron transfer from the CB of Bi_2S_3 to that of FeOOH. Then the photo-generated electrons transferred to ITO electrode producing excellent photocurrent signal. Meanwhile, the modification of Au NPs obviously enhanced the photocurrent intensity. On the one hand, the SPR effect of Au NPs prompted electrons injected to CB of Bi_2S_3 and FeOOH. On the other hand, the great conductivity of Au NPs significantly improved the photoelectric conversion efficiency. In addition, the oxidation potentials of {Mo_{368}} were 0.039 V and 0.27 V (vs SCE), which would be oxidized rapidly by the photo-generated holes of FeOOH (E^0 = 2.78 V) or Bi_2S_3 (E^0 = 1.64 V) (Zhao et al., 2012). Therefore, {Mo_{368}} was designed as an ideal electron donor to capture the photo-generated holes ensuring the stability of the platform on the whole process.

3.3. Optimization of experimental conditions

The deposition time of PB exerted an important effect on the thickness of FeOOH, which influenced the activity of PEC sensor. If FeOOH loaded on the electrode became too thin, the photocurrent intensity could be weak. And the excessively thick FeOOH could fall off and result in the unstable signal. Hence, the deposition time of PB was optimized under the same conditions (Fig. S2A). It was obvious that the PEC sensor showed the optimal performance when the deposition time was 400 s. In addition, after excess {Mo_{368}} was dissolved in PBS solution, the solution turned into mazarine solution that generated a certain absorption to visible light. As an electrolyte, the competitive absorption between {Mo_{368}} and matrix material to visible light hindered electron transfer and reduced the photocurrent intensity. And the insufficient {Mo_{368}} could not guarantee the stability of the whole PEC sensor. Therefore, the effect of various concentration of {Mo_{368}} on the photocurrent intensity of PEC sensor was measured and showed in Fig. S2B. The result indicated that 0.02 mg mL^{-1} of {Mo_{368}} was optimal. Moreover, the appropriate pH of electrolyte was explored because overly acidic or basic environment both influenced the existing form of {Mo_{368}}. It was shown in Fig. S2C that the suitable pH value was about 6.24.

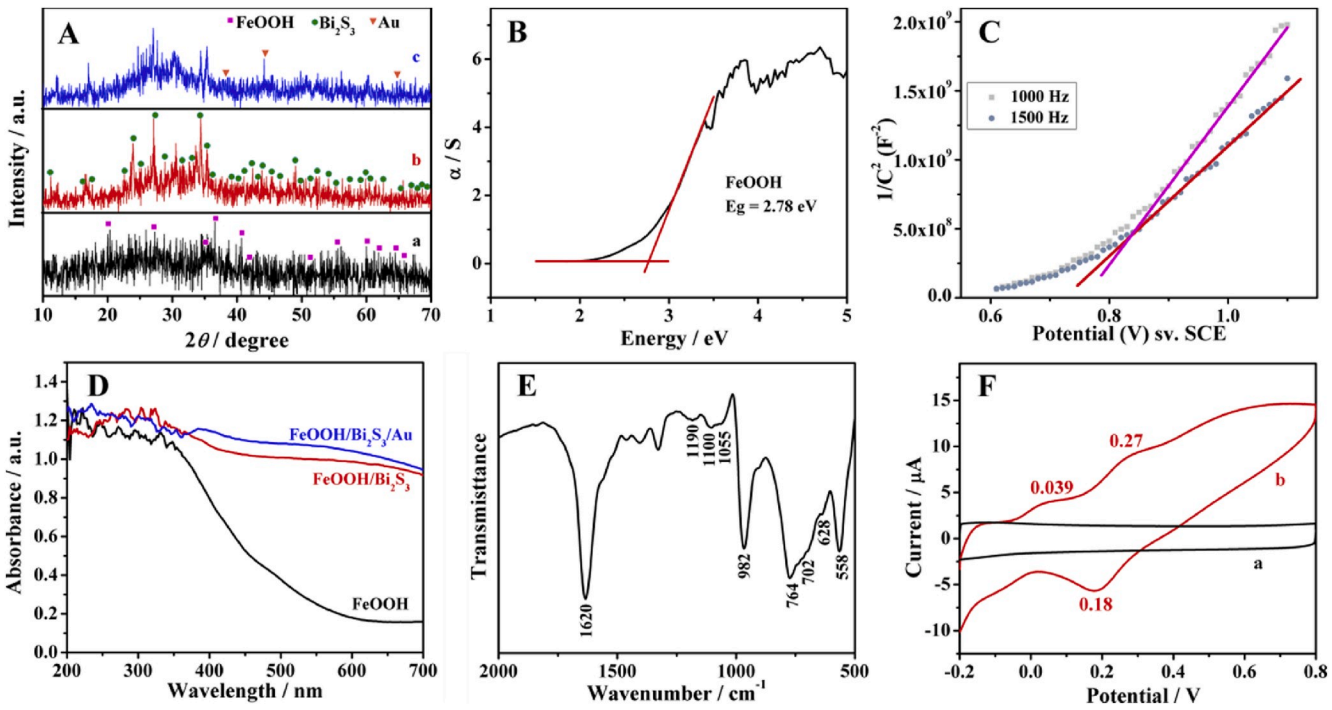

Fig. 2. (A) XRD patterns of FeOOH (a), $FeOOH/Bi_2S_3$ (b), $FeOOH/Bi_2S_3/Au$ (c). (B) UV–vis diffuse reflectance spectrum and (C) Mott-Schottky curves of FeOOH. (D) UV–vis diffuse reflectance spectra of FeOOH, $FeOOH/Bi_2S_3$, $FeOOH/Bi_2S_3/Au$. (E) FT-IR spectrum of $\{Mo_{368}\}$. (F) After filling with nitrogen for 20 min, the CV curves of ITO electrode using PBS solution with (b) or without $\{Mo_{368}\}$ (a) as electrolyte.

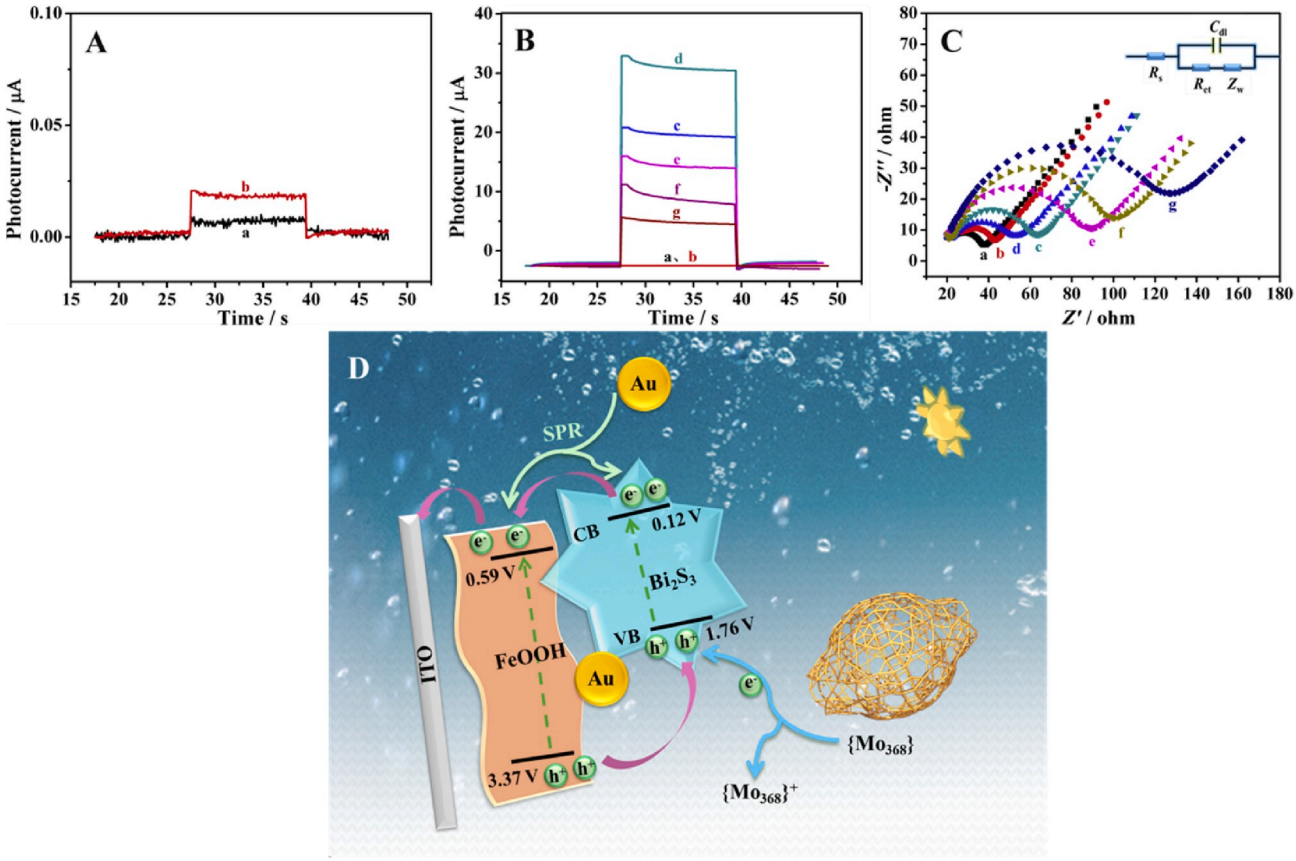

Fig. 3. (A) and (B) Photocurrent response curves and (C) EIS Nyquist plots of (a) ITO, (b) ITO/FeOOH, (c) $ITO/FeOOH/Bi_2S_3$, (d) $ITO/FeOOH/Bi_2S_3/Au$, (e) $ITO/FeOOH/Bi_2S_3/Au$/anti-cTnI, (f) $ITO/FeOOH/Bi_2S_3/Au$/anti-cTnI/BSA and (g) $ITO/FeOOH/Bi_2S_3/Au$/anti-cTnI/BSA/cTnI. The inset of C was related Randles equivalent circuit. (D) Electron transfer mechanism of the constructed PEC sensor (The structure of $\{Mo_{368}\}$ was reprinted from *Polyhedron*. 2004, 23, 2381-2385). The used potential was 0 V.

3.4. The performance analysis of designed PEC sensor

The performance of the designed PEC sensor was tested under the optimal conditions. The various concentrations of cTnI exhibited different photocurrent signals and the trend was showed in Fig. 4A. Moreover, Fig. 4B displayed the corresponding logarithmic calibration curve in the concentration range of 1.00 pg mL^{-1} - 100 ng mL^{-1}. And the regression equation and linear coefficient were I (μA) = 5.695–0.9697 log (c_{cTnI}, ng·mL^{-1}) and 0.998, respectively. According to the previous report(Ren et al., 2015), the detection limit was calculated to be 0.76 pg mL^{-1}. The proposed PEC sensor had superior performance compared with other reported methods in Table S2 (the details were shown in the Supporting Information), and possessed great application potential.

For an excellent PEC sensor, satisfactory stability, selectivity and reproducibility were essential. Under repeated on/off visible light illumination, there was no significant change of the photocurrent signal in Fig. 4C (c_{cTnI} = 1 ng mL^{-1}). In addition, the selectivity test was implemented and displayed in Fig. 4D. Whether or not the electrodes contained interferents that squamous cell carcinoma antigen (SCCA), brain natriuretic peptide (BNP) and procalcitonin (PCT), there were no significant changes in photocurrent signals (the blank electrode represented the ITO/FeOOH/Bi_2S_3/Au/anti-cTnI/BSA electrode). Besides, the reproducibility evaluation of the proposed PEC sensor (c_{cTnI} = 1 ng mL^{-1}) was investigated utilizing five electrodes. Under the same conditions, the five electrodes were prepared and detected (shown in Fig. S3), and then the relative standard deviation (RSD) was about 4.7%. Based on the above results, it was obvious that the constructed PEC sensor possessed the great stability, selectivity and reproducibility.

3.5. Real sample analysis

Using the standard addition method, various concentrations of cTnI were added into the diluted human serum samples to measure recoveries and analyze the practicability of the designed PEC sensor. As observed from Table 1, the calculated RSD of the proposed PEC sensor was less

Table 1
The results of the cTnI determination in human serum sample.

Initial content of cTnI in serum (pg·mL^{-1})	The addition content (pg·mL^{-1})	The detection content (pg·mL^{-1},n = 5)	RSD (%, n = 5)	Recovery (%)
28.90	25.00	54.28, 54.74, 52.45, 55.97, 53.10	2.558	100.8
	30.00	59.14, 60.51, 56.54, 57.42, 55.18	3.645	96.20
	40.00	67.12, 66.39, 70.46, 66.55, 71.13	3.334	98.58

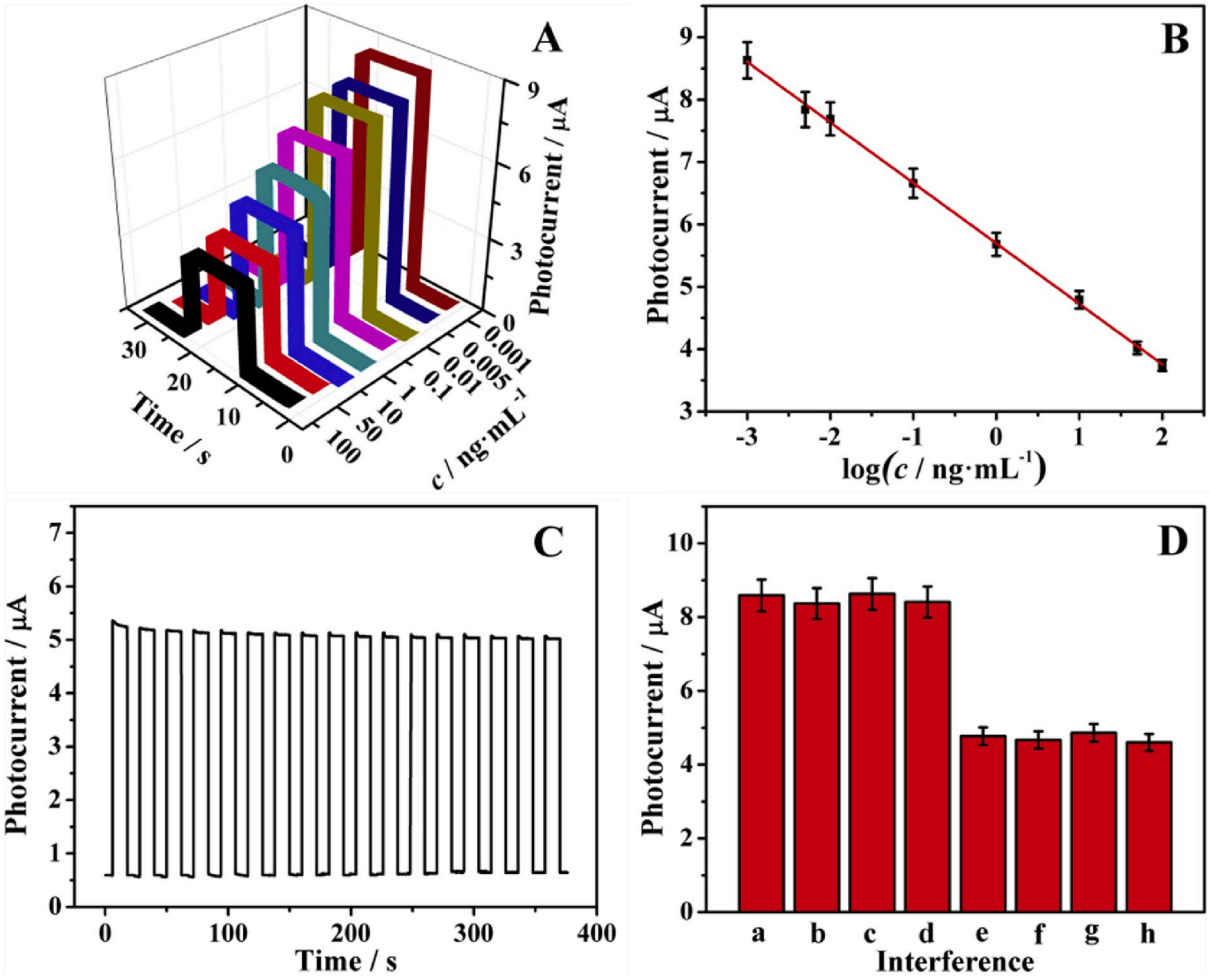

Fig. 4. The corresponding (A) current responses and (B) calibration curve of the designed PEC sensor with difference concentrations of cTnI. (C) Stability analysis of the designed PEC sensor under repeated on/off visible light illumination (c_{cTnI} = 1 ng mL^{-1}). (D) Selectivity test of the designed PEC sensor. (a) Blank, (b) Blank + 100 ng mL^{-1} SCCA, (c) Blank + 100 ng mL^{-1} BNP, (d) Blank + 100 ng mL^{-1} PCT, (e) 1 ng mL^{-1} cTnI, (f) 1 ng mL^{-1} cTnI + 100 ng mL^{-1} SCCA, (g) 1 ng mL^{-1} cTnI + 100 ng mL^{-1} BNP, (h) 1 ng mL^{-1} cTnI + 100 ng mL^{-1} PCT. The applied potential was 0 V.

than 3.7%, while the range of recovery was from 96.20 to 100.8%. Moreover, the *F*-test and *t*-test were utilized to analyze the error between the ELISA method and designed PEC sensor (shown in Table S3). While the confidence coefficient α was 0.05, the calculated *F* was less than F_f (F = 1.48, F_f = 6.39) and the *t* value was less than $t_{\alpha,\ f}$ (t = 0.133, $t_{\alpha,\ f}$ = 2.31), which strongly proved the error was negligible between the above methods, and the designed PEC sensor owned excellent feasibility and veracity.

4. Conclusion

A novel PEC sensor is proposed to sensitively detect cTnI, while the unique {Mo_{368}} is designed as electron donor. With perfect morphology and interesting electronic characteristics, {Mo_{368}} ensures the stability of the whole electron transfer process. In addition, FeOOH prepared by a simple operation contains abundant active hydroxyl groups. By the adsorption between positive and negative ion, Bi_2S_3 is utilized to sensitize FeOOH for accelerating the electron transfer. And the SPR effect and outstanding optical stability of Au NPs further improve the photoelectric conversion efficiency, achieving the sensitive detection of cTnI in early diagnosis of cardiovascular disease. The proposed PEC sensor provides an interesting and novel strategy for the design of sensor. Meanwhile, the exact reaction mechanism of {Mo_{368}} needs further exploration.

Declaration of competing interest

The authors declare that they have no known competing financial interests or personal relationships that could have appeared to influence the work reported in this paper.

CRediT authorship contribution statement

Chunzhu Bao: Conceptualization, Data curation. **Xin Liu:** Writing - review & editing, Methodology. **Xinrong Shao:** Formal analysis. **Xiang Ren:** Formal analysis. **Yong Zhang:** Formal analysis. **Xu Sun:** Formal analysis. **Dawei Fan:** Writing - review & editing, Methodology, Data curation. **Qin Wei:** Funding acquisition, Formal analysis. **Huangxian Ju:** Funding acquisition, Formal analysis.

Acknowledgments

This research was financially supported by the Innovation team project of colleges and universities in Jinan (No.2019GXRC027), the National Key Scientific Instrument and Equipment Development Project of China (No. 21627809), the National Natural Science Foundation of China (Nos. 21505051, 21575050, 21777056), the Jinan Scientific Research Leader Workshop Project (2018GXRC024).

Appendix A. Supplementary data

Supplementary data to this article can be found online at https://doi.org/10.1016/j.bios.2020.112157.

References

Adhikary, S.D., Tiwari, A., Nagaiah, T.C., Mandal, D., 2018. ACS Appl. Mater. Interfaces 10, 38872–38879.
Ai, Y., Liu, L., Zhang, C., Qi, L., He, M., Liang, Z., Sun, H.B., Luo, G., Liang, Q., 2018. ACS Appl. Mater. Interfaces 10, 32180–32191.
Bao, C., Fan, D., Liu, X., Wang, X., Wu, D., Ma, H., Hu, L., Wang, H., Sun, X., Wei, Q., 2019. Biosens. Bioelectron. 142, 111513–111519.
Cao, J.T., Wang, B., Dong, Y.X., Wang, Q., Ren, S.W., Liu, Y.M., Zhao, W.W., 2018. ACS Sens. 3, 1087–1092.
Chapman, A.R., Lee, K.K., McAllister, D.A., Cullen, L., Greenslade, J.H., Parsonage, W., Worster, A., Kavsak, P.A., Blankenberg, S., Neumann, J., Sörensen, N.A., Westermann, D., Buijs, M.M., Verdel, G.J.E., Pickering, J.W., Than, M.P., Twerenbold, R., Badertscher, P., Sabti, Z., Mueller, C., Anand, A., Adamson, P., Strachan, F.E., Ferry, A., Sandeman, D., Gray, A., Body, R., Keevil, B., Carlton, E., Greaves, K., Korley, F.K., Metkus, T.S., Sandoval, Y., Apple, F.S., Newby, D.E., Shah, A.S.V., Mills, N.L., 2017. J. Am. Med. Assoc. 318, 1913–1924.
Chen, J., Kong, L., Sun, X., Feng, J., Chen, Z., Fan, D., Wei, Q., 2018. Biosens. Bioelectron. 117, 340–346.
Chen, Y., Wang, G., Li, H., Zhang, F., Jiang, H., Tian, G., 2019. J. Colloid Interface Sci. 555, 214–223.
Chi, H., Han, Q., Chi, T., Xing, B., Ma, N., Wu, D., Wei, Q., 2019. Biosens. Bioelectron. 132, 1–7.
Cui, L., Hu, J., Wang, M., Diao, X.K., Li, C.C., Zhang, C.Y., 2018. Anal. Chem. 90, 11478–11485.
Fan, D., Bao, C., Khan, M., Wang, C., Zhang, Y., Liu, Q., Zhang, X., Wei, Q., 2018a. Biosens. Bioelectron. 106, 14–20.
Fan, D., Bao, C., Liu, X., Wu, D., Zhang, Y., Wang, H., Du, B., Wei, Q., 2018b. J. Mater. Chem. B 6, 7634–7642.
Feng, J.X., Ye, S.H., Xu, H., Tong, Y.X., Li, G.R., 2016. Adv. Mater. 28, 4698–4703.
Gao, C., Xue, J., Zhang, L., Zhao, P., Cui, K., Ge, S., Yu, J., 2019. Biosens. Bioelectron. 131, 17–23.
Garai, S., Merca, A., Bhowmik, S., El Moll, H., Li, H., Haso, F., Nogueira, H., Liu, T., Wu, L., Gouzerh, P., Muller, A., 2015. Soft Matter 11, 2372–2378.
Guo, S.-X., Li, F., Chen, L., MacFarlane, D.R., Zhang, J., 2018. ACS Appl. Mater. Interfaces 10, 12690–12697.
Guo, Y., Ao, Y., Wang, P., Wang, C., 2019. Appl. Catal., B 254, 479–490.
Han, L., Bai, L., Dong, S., 2014. Chem. Commun. (Cambridge, U. K.) 50, 802–804.
Hu, Y., Yang, H., Chen, J., Xiong, T., Balogun, M.J.T., Tong, Y., 2019. ACS Appl. Mater. Interfaces 11, 5152–5158.
Jia, Y., Yang, L., Xue, J., Zhang, N., Fan, D., Ma, H., Ren, X., Hu, L., Wei, Q., 2019. ACS Sens. 4, 1909–1916.
Leung, K.K., Yu, H.Z., Bizzotto, D., 2019. ACS Sens. 4, 513–520.
Li, Y., Chen, F., Luan, Z., Zhang, X., 2018. Biosens. Bioelectron. 119, 63–69.
Li, H., Wang, J., Wang, X., Lin, H., Li, F., 2019a. ACS Appl. Mater. Interfaces 11, 16958–16964.
Li, M., Liang, W., Yuan, R., Chai, Y., 2019b. ACS Appl. Mater. Interfaces 11, 11834–11840.
Li, S., Wang, Z., Zhang, X., Zhao, J., Hu, Z., Wang, Z., Xie, X., 2019c. Chem. Eng. J. 378, 122169.
Li, X.X., Liu, J., Zhang, L., Dong, L.Z., Xin, Z.F., Li, S.L., Huang-Fu, X.Q., Huang, K., Lan, Y.Q., 2019d. ACS Appl. Mater. Interfaces 11, 25790–25795.
Li, Y., Li, X., Meng, Y., Hun, X., 2019e. Biosens. Bioelectron. 130, 269–275.
Li, Z., Zhou, X., Yang, J., Fu, B., Zhang, Z., 2019f. ACS Appl. Mater. Interfaces 11, 21417–21423.
Lv, S., Zhang, K., Zeng, Y., Tang, D., 2018. Anal. Chem. 90, 7086–7093.
Lv, H., Li, Y., Zhang, X., Li, X., Xu, Z., Chen, L., Li, D., Dong, Y., 2019. Biosens. Bioelectron. 133, 72–78.
Müller, A., Botar, B., Das, S.K., Bögge, H., Schmidtmann, M., Merca, A., 2004. Polyhedron 23, 2381–2385.
Müller, A., Eike, B., Hartmut, B.G., Marc, S., Andreas, D., 2010. Angew. Chem. Int. Ed. 41, 1162–1167.
Paul, S., Ghosh, S., Barman, D., De, S.K., 2017. Appl. Catal., B 219, 287–300.
Ren, K., Wu, J., Yan, F., Zhang, Y., Ju, H., 2015. Biosens. Bioelectron. 66, 345–349.
Saha, S., Chan, Y., Soleymani, L., 2018. ACS Appl. Mater. Interfaces 10, 31178–31185.
Sun, D., Lin, X., Lu, J., Wei, P., Luo, Z., Lu, X., Chen, Z., Zhang, L., 2019a. Biosens. Bioelectron. 142, 111578.
Sun, D., Luo, Z., Lu, J., Zhang, S., Che, T., Chen, Z., Zhang, L., 2019b. Biosens. Bioelectron. 134, 49–56.
Szunerits, S., Mishyn, V., Grabowska, I., Boukherroub, R., 2019. Biosens. Bioelectron. 131, 287–298.
Tan, Y., Wang, Y., Li, M., Ye, X., Wu, T., Li, C., 2017. Biosens. Bioelectron. 91, 741–746.
Wang, H.-N., Zhang, M., Zhang, A.M., Shen, F.-C., Wang, X.-K., Sun, S.-N., Chen, Y.-J., Lan, Y.-Q., 2018a. ACS Appl. Mater. Interfaces 10, 32265–32270.
Wang, S., Lan, H., Liu, H., Qu, J., 2016. Phys. Chem. Chem. Phys. 18, 9437–9445.
Wang, Y., Cao, X., Hu, Q., Liang, X., Tian, T., Lin, J., Yue, M., Ding, Y., 2019. ACS Appl. Mater. Interfaces 11, 23135–23143.
Wang, Y., Jin, J., Chu, W., Cahen, D., He, T., 2018b. ACS Appl. Mater. Interfaces 10, 15304–15313.
Welsh, P., Preiss, D., Hayward, C., Shah, A.S.V., McAllister, D., Briggs, A., Boachie, C., McConnachie, A., Padmanabhan, S., Welsh, C., Woodward, M., Campbell, A., Porteous, D., Mills, N.L., Sattar, N., 2019. Circulation 139, 2754–2764.
Wen, S., Miao, X., Fan, G.C., Xu, T., Jiang, L.P., Wu, P., Cai, C., Zhu, J.J., 2019. ACS Sens. 4, 301–308.
Xin, F., Jia, Y., Sun, J., Dang, L., Liu, Z., Lei, Z., 2018. ACS Appl. Mater. Interfaces 10, 32192–32200.
Yuan, H., Ji, W., Chu, S., Liu, Q., Qian, S., Guang, J., Wang, J., Han, X., Masson, J.F., Peng, W., 2019. ACS Sens. 4, 704–710.
Zhao, W.W., Ma, Z.Y., Yan, D.Y., Xu, J.J., Chen, H.Y., 2012. Anal. Chem. 84, 10518–10521.
Zhou, Q., Lin, Y., Shu, J., Zhang, K., Yu, Z., Tang, D., 2017. Biosens. Bioelectron. 98, 15–21.
Zhou, Q., Xue, H., Zhang, Y., Lv, Y., Li, H., Liu, S., Shen, Y., Zhang, Y., 2018. ACS Sens. 3, 1385–1391.